
Hybrid Adversarial Inverse Reinforcement Learning

Mingqi Yuan^{1,2} Man-on Pun^{1,2,3} Yi Chen^{1,2}

¹The Chinese University of Hong Kong, Shenzhen

²Shenzhen Research Institute of Big Data

³Shenzhen Key Laboratory of IoT Intelligent System and Wireless Network Technology

mingqiyuan@link.cuhk.edu.cn

{simonpun,yichen}@cuhk.edu.cn

Abstract

Extrapolating beyond-demonstrator (BD) through the inverse reinforcement learning (IRL) algorithm aims to learn from and outperform the demonstrator. In sharp contrast to the conventional reinforcement learning (RL) algorithms, BD-IRL can overcome the dilemma incurred in the reward function design and improve the exploration mechanism of RL, which opens new avenues to building superior expert systems. Most existing BD-IRL algorithms are performed in two stages by first inferring a reward function before learning a policy via RL. However, such two-stage BD-IRL algorithms suffer from high computational complexity, weak robustness, and large performance variations. In particular, a poor reward function derived in the first stage will inevitably incur severe performance loss in the second stage. In this work, we propose a hybrid adversarial inverse reinforcement learning (HAIRL) algorithm that is one-stage, model-free, generative-adversarial (GA) fashion and curiosity-driven. Thanks to the one-stage design, the HAIRL can integrate both the reward function learning and the policy optimization into one procedure, which leads to many advantages such as low computational complexity, high robustness, and strong adaptability. More specifically, HAIRL simultaneously imitates the demonstrator and explores BD performance by utilizing hybrid rewards. In particular, the Wasserstein-1 distance (WD) is introduced into HAIRL to stabilize the imitation procedure while a novel end-to-end curiosity module (ECM) is developed to improve the exploration. Finally, extensive simulation results confirm that HAIRL can achieve higher performance as compared to other similar BD-IRL algorithms. Our code is available at our GitHub website ¹.

1 Introduction

Reinforcement learning (RL) has been widely applied in building expert systems (e.g., AlphaZero and AlphaStar) due to its superior learning and exploration ability [1, 2]. But it is also increasingly showing its critical limitations in practice. In RL, the agent learns policies for specific objective tasks by maximizing the expected cumulative rewards in the long run. However, the reward signal is usually sparse or even missing in many real-world scenarios, and it is analytically intractable to construct a shaped reward function [3]. In addition, many RL algorithms suffer from imperfect exploration mechanisms, in which the agent is easy to fall into local optima [4]. Techniques like entropy-regularized reward only improve the exploration of actions for a given state, but it is insufficient for the agent to comprehend the environment better.

To cope with the aforementioned problem related to the reward function design, the inverse reinforcement learning (IRL) is developed to infer a reward function from demonstrations provided by a

¹<https://github.com/yuanmingqi/HAIRL>

demonstrator [5]. For instance, a sophisticated driver is considered to possess some driving skills. The IRL formulates such skills as an explicit reward function so that a new driver can use this reward function to establish his driving policy. Based on the inferred reward function, the policy of the demonstrator can be recovered via RL [6]. However, such learned policy is consistently found to be sub-optimal and unable to outperform the demonstrator [7]. This is because the IRL only aims to find the reward function that makes the demonstrations appear optimal, without making any efforts to further improve the policy [8]. To outperform the demonstrator, a stronger reward function that comprehends the environment better is needed.

Learning from and outperforming the demonstrator via IRL is commonly referred to as beyond-demonstrator (BD) IRL in the literature. The concept of extrapolating BD performance via IRL was first proposed in [7] by designing a trajectory-ranking reward extrapolation (TREX) framework. More specifically, TREX first collects a series of ranked trajectories before training a parameterized reward function that matches the rank relation. Finally, the reward function is employed to learn a policy via RL. By fully exploring the reward space, TREX provides a high-quality reward function to learn BD policies. In [9], TREX was further extended to the multi-agent task. Since it is impractical to get well-ranked trajectories for TREX, [10] proposed a disturbance-based reward extrapolation (DREX) framework, which can automatically generate the ranked demonstrations by injecting noise into a policy learned through behavioral cloning. However, both TREX and DREX are hindered by the necessity of abundant demonstrations. To address this problem, [8] proposed a generative intrinsic reward-driven imitation learning (GIRIL) framework, which takes a one-life demonstration to learn a family of reward functions using variational autoencoder (VAE) [11]. In particular, [8] first introduced the curiosity module (CM) to the BD-IRL to explore the BD performance. Simulation results showed that the GIRIL can learn a BD policy at the cost of fewer demonstrations. Despite their many advantages, all the algorithms discussed above are divided into two separate stages in which a reward function is first learned before the BD policy is explored via RL. As a result, they suffer from high computational complexity and unstable performance. In particular, a poor reward function derived in the first stage would inevitably incur severe performance loss in the second stage.

Inspired by the discussions above, we consider building a unified one-stage BD-IRL algorithm that simultaneously learns the reward function and optimizes the policy. To our best knowledge, this is the first one-stage BD-IRL framework reported in the literature. In our one-stage algorithm, the reward function is updated dynamically to adapt to the varying learning process, enabling better generalization and robustness. Moreover, it can significantly reduce the computational complexity, since the reward function and the policy are obtained simultaneously within one training process. In this paper, we propose the hybrid adversarial inverse reinforcement learning (HAIRL), which is a model-free, one-stage, GA fashion and curiosity-driven IRL algorithm. The HAIRL uses two independent modules for behavior imitation and policy exploration, namely the extrinsic reward block (ERB) and intrinsic reward block (IRB). Simulation results show that HAIRL outperforms the conventional BD-IRL algorithms.

2 Related Work

Inverse reinforcement learning. The dilemma in the reward function design promotes the development of IRL. IRL aims to find a reward function that explains the demonstrations drawn from an expert [5]. Given the inferred reward function, the expert policy can be recovered via RL [6]. Many IRL algorithms have been developed both for single-agent and multi-agent tasks based on deep learning, information theory and probability theory and so on [12, 13, 14, 15, 16, 17, 18, 19]. For instance, the maximum entropy (ME)-IRL seeks to find a reward function that makes the demonstrations satisfy the principle of ME [12]. More specifically, ME-IRL assumes that the probability of choosing a trajectory is proportional to the sum of the rewards along the trajectory. Finally, ME-IRL learns the reward function using the maximum likelihood estimation (MLE). However, these methods only seek a reward function that matches the demonstrations. As a result, they were *not* designed to outperform the demonstrator.

Based on the ME assumption, [20] proved the connection and equivalence between IRL and GA network (GAN) [21]. Furthermore, [22] subsequently proposed the adversarial IRL (AIRL) that solves the IRL problem using GA fashion. In AIRL, the agent serves as the generator to produce trajectories while the discriminator classifies the trajectories as either from the generator or from the expert. The discriminator score is utilized as the reward to train the agent to imitate the expert.

In particular, AIRL obtains the reward function and recovers policy simultaneously, which has low computational complexity and high robustness. In our work, we inherit the idea of AIRL and redesign the reward module to build the one-stage BD-IRL algorithm.

Curiosity-driven reinforcement learning. Our work is also inspired by the research on the curiosity-driven RL. There are two kinds of reward signal in RL, namely the extrinsic reward signal (ERS) and intrinsic reward signal (IRS) [23]. ERS is usually given by the environment explicitly, such as the time cost in the Mountain-Car game. In contrast, IRS represents the intrinsic learning motivation or curiosity of the agent, which is an implicit and abstract concept. Many prior works have been devoted to characterizing IRS, and these methods can be categorized into two approaches. More specifically, one approach focuses on encouraging the agent to visit those novel states [24, 25] while the other drives the agent to reduce the uncertainty in predicting the consequence of its own actions [26, 27, 28, 4]. Despite their discrepancy, both approaches encourage the agent to fully explore the environment, increasing the probability of achieving higher performance. In [29], the first practical and general module entitled intrinsic curiosity module (ICM) was proposed using an attendant model. More specifically, this model first predicts the next state using the current state-action pair from a given transition. After that, the prediction error taken as IRS is added with ERS to form a mixed reward. In particular, [30] proves that the agent can learn a policy of considerably good performance using only IRS in extensive experiments. In this work, we propose a novel end-to-end curiosity module (ECM) with simplified architecture for our framework to achieve improved exploration and BD performance.

3 Problem Formulation

We study the BD-IRL problem considering the Markov decision process (MDP) defined by a tuple $\mathcal{M} = \langle \mathcal{S}, \mathcal{A}, \mathcal{T}, r^*, \rho(s_0), \gamma \rangle$, where \mathcal{S} is the state space, \mathcal{A} is the action space, $\mathcal{T}(s'|s, a)$ is the transition distribution, $r^* : \mathcal{S} \times \mathcal{A} \rightarrow \mathbb{R}$ is the true reward function, $\rho(s_0)$ is the initial state distribution, and $\gamma \in (0, 1]$ is a discount factor. Note that r^* is solely determined by the environment and the task. Furthermore, we denote by $\pi(a|s)$ the policy of the agent. In each step, the agent observes the state of environment before selecting an action from the action space. After that, the state-action pair will be evaluated by the reward function. Next, we will first define the objective of the RL based on the MDP structure.

Definition 1 (RL). *Given MDP \mathcal{M} , the objective of RL is to find the optimal policy π^* that maximizes the expected discounted return:*

$$\pi^* = \operatorname{argmax}_{\pi \in \Pi} J(\pi|r^*), \quad (1)$$

where $J(\pi|r^*) = \mathbb{E}_{\tau \sim \pi} \sum_{t=0}^{T-1} \gamma^t r_t^*(s_t, a_t)$, Π is the set of all stationary policies, and $\tau = (s_0, a_0, \dots, a_{T-1}, s_T)$ is the trajectory generated by the policy.

On the contrary, the conventional IRL aims to learn a reward function that explains the observed behaviors [5]. Given a set of trajectories $\mathcal{D} = \{\tau_1, \dots, \tau_N\}$ drawn from a demonstrator, the corresponding IRL problem can be defined as:

Definition 2 (IRL). *Given MDP \mathcal{M} and a set of trajectories $\mathcal{D} = \{\tau_1, \dots, \tau_N\}$, the objective of IRL can be formulated as solving a MLE problem [12]:*

$$\max_{\theta} \mathbb{E}_{\tau \sim \mathcal{D}} [\log p_{\theta}(\tau)], \quad (2)$$

where $p_{\theta}(\tau) \propto \rho(s_0) \prod_{t=0}^{T-1} \mathcal{T}(s_{t+1}|s_t, a_t) e^{\gamma^t r_{\theta}(s_t, a_t)}$, and $r_{\theta}(s_t, a_t)$ is the parameterized reward function.

Such objective simply aims to imitate the policy of the demonstrator, which can not learn a BD policy. In this paper, we aim to obtain a BD policy through the IRL. Denote by $\hat{\pi}$ the generation policy, we say that $\hat{\pi}$ outperforms the demonstrator if:

$$J(\hat{\pi}|r^*) > J(\mathcal{D}|r^*) = \frac{1}{|\mathcal{D}|} \sum_{\tau \in \mathcal{D}} J(\tau|r^*), \quad (3)$$

where $J(\tau|r^*) = \sum_{(s_t, a_t) \in \tau} \gamma^t r^*(s_t, a_t)$, $J(\mathcal{D}|r^*)$ is the estimation of the expected discounted return of the demonstrator.

It is intractable to straightforwardly obtain the optimal generation policy $\hat{\pi}$. The following section proposes a one-stage BD-IRL algorithm, which learns a hybrid reward function and realizes both the imitation and BD performance within a unified architecture.

4 Hybrid Adversarial Inverse Reinforcement Learning

In this section, we propose a HAIRL framework that is a one-stage, model-free, GA fashion, and curiosity-driven IRL framework. As illustrated in Fig. 1, the architecture of HAIRL is composed of two major components, namely ERB and IRB. ERB generates an ERS based on the demonstrations through GA fashion, which drives the agent to approach the demonstrator policy rapidly. Meanwhile, IRB generates an IRS using curiosity module, leading the agent to further explore for the BD performance. Finally, ERS and IRS form a hybrid reward for policy updates. The two components are elaborated in detail in the following.

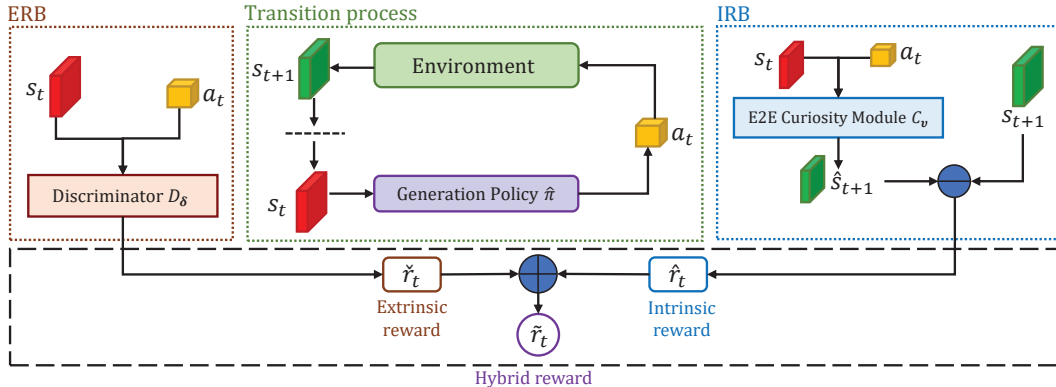


Figure 1: The architecture of HAIRL where \oplus denotes the add operation and \ominus denotes the Euclidean distance.

4.1 Extrinsic Reward Block

We propose to build ERB following the GA approach proposed in AIRL [22]. In a standard GA structure, a generator is employed to capture the true data distribution while a discriminator is utilized to estimate the probability that a sample belongs to the true data, rather than the generated data [21]. However, the conventional GA structure suffers from two critical drawbacks. First, the discriminator is trained using the binary cross-entropy as the loss function, which can not accurately reflect the distance between the true and generated data distributions. As a result, the conventional GA structure may lead to the gradient vanishing of the generator. In addition, [31] has shown that the conventional loss function is ambiguous for the generator, which potentially leads to model collapse.

To cope with these problems, we introduce the Wasserstein-1 distance (WD) to design ERB in a manner similar to the popular Wasserstein GAN proposed in [32]. In sharp contrast to the conventional loss function, WD can measure the distance between any two data distributions. As a result, WD can provide more stable gradients to overcome model collapse and improve model generalization. We first formally define WD as follows:

Definition 3 (WD). Let P_r, P_g be two probability distributions defined on a compact set \mathcal{X} . Then, the WD between P_r and P_g is defined as [32]:

$$W(P_r, P_g) = \inf_{P_c \sim \Gamma(P_r, P_g)} \mathbb{E}_{(x, y) \sim P_c} [||x - y||], \quad (4)$$

where $\Gamma(P_r, P_g)$ is the set of all joint distributions whose marginals are P_r and P_g , respectively.

Since it is non-trivial to directly evaluate Eq. (4), WD can be transformed into a computable form based on the Kantorovich-Rubinstein duality as follows [33]:

$$\begin{aligned} W(P_r, P_g) &= \sup_{\|f\|_L \leq 1} \mathbb{E}_{x \sim P_r} [f(x)] - \mathbb{E}_{x \sim P_g} [f(x)] \\ &\approx \max_{\|f\|_L \leq 1} \mathbb{E}_{x \sim P_r} [f(x)] - \mathbb{E}_{x \sim P_g} [f(x)], \end{aligned} \quad (5)$$

where $f : \mathcal{X} \rightarrow \mathbb{R}$ is the 1-Lipschitz function. Therefore, we can construct a family of parameterized functions to approximate the supremum. In practice, such functions can be represented as a deep neural network (DNN).

We represent the discriminator D_δ by a DNN with parameters δ with δ being clipped into the range of $[-\zeta, \zeta]$ to satisfy the Lipschitz condition for $\zeta \in \mathbb{R}^+$. In ERB, the generation policy $\hat{\pi}$ serves as the generator, interacting with the environment to produce trajectories. Given a trajectory $\tau = (s_0, a_0, \dots, a_{T-1}, s_T)$, denote by $\hat{\pi}(\tau) = \rho(s_0) \prod_{t=0}^{T-1} \mathcal{T}(s_{t+1}|s_t, a_t) \hat{\pi}(a_t|s_t)$ the trajectory distribution induced by the $\hat{\pi}$, the discriminator is trained to minimize the following loss function to approximate the $W(\mathcal{D}, \hat{\pi}(\tau))$:

$$L(\delta) = \sum_{t=0}^{T-1} \mathbb{E}_{\hat{\pi}(\tau)}[D_\delta(s_t, a_t)] - \sum_{t=0}^{T-1} \mathbb{E}_{\mathcal{D}}[D_\delta(s_t, a_t)]. \quad (6)$$

To minimize the WD between \mathcal{D} and $\hat{\pi}(\tau)$, we define an ERS denoted by \check{r} for the generation policy:

$$\check{r}_\delta(s_t, a_t) = \mathbb{E}_{\hat{\pi}(\tau)}[D_\delta(s_t, a_t)]. \quad (7)$$

More specifically, we prove that the demonstrator policy can be learned by optimizing Eq. (1) using Eq. (7), which leads to the following theorem:

Theorem 1 (Consistency). *Given MDP \mathcal{M} and a set of trajectories $\mathcal{D} = \{\tau_1, \dots, \tau_N\}$, the demonstrator policy can be learned by minimizing the loss function Eq. (6) while maximizing the discounted return with the reward function shown in Eq. (7).*

Proof. See the proof in Appendix A. □

Since ERB learns from the sampled trajectories, its performance is inevitably influenced by the quantity and quality of the trajectories. Regardless of the BD objective, ERB can be regarded as an independent IRL algorithm for imitating the demonstrator. Most existing IRL works barely discussed the sample complexity of the algorithm. Here we introduce the following theorem to analyze the sample complexity of our ERB. Since ERB actually minimizes the WD between \mathcal{D} and $\hat{\pi}(\tau)$, we only need to analyze the sample complexity of minimizing the WD.

Theorem 2 (Sample Complexity). *Given a set of trajectories $\mathcal{D} = \{\tau_1, \dots, \tau_N\}$, with probability at least $1 - \kappa$, ERB recovers a policy $\hat{\pi}$ such that:*

$$\max_{\|f\|_L \leq 1} \mathbb{E}_{(s,a) \sim \mathcal{D}}[f(s, a)] - \mathbb{E}_{(s,a) \sim \hat{\pi}(\tau)}[f(s, a)] \leq 4\sqrt{\frac{2 \ln(|\Pi|) - \ln(\kappa)}{M}}, \quad (8)$$

where f is the Lipschitz-1 function, M is the number of the state-action pairs in \mathcal{D} , and $|\Pi|$ is the cardinality of the policy set.

Proof. See the proof in Appendix B □

Theorem 2 indicates that the left-hand side of the inequality is independent on the form of f . It is only determined by the cardinality of the policy set and sample set. Given a policy set, Theorem 2 also shows that more samples make the imitation more accurate.

4.2 Intrinsic Reward Block

Through ERS, the generation policy can rapidly approach the demonstrator policy. Meanwhile, the agent is expected to extrapolate the BD performance by further exploring the environment. We propose to introduce CM to provide IRS for the agent to encourage exploration. Fig. 2 illustrates the architecture of ICM and ECM. Both ICM and ECM generate IRS based on the uncertainty for the agent to predict the consequence of its own actions. In ICM, IRS is defined as the square of the Euclidean distance (ED) between the encoded true next state $\omega(s_{t+1})$ and the encoded predicted next state $\omega(\hat{s}_{t+1})$ where $\omega(\cdot)$ is an encoding function. Such a design encourages the agent to visit the infrequently-seen state-action pairs, which prevents the agent from falling into the local optima. As a result, the proposed agent can achieve a better performance at a higher probability.

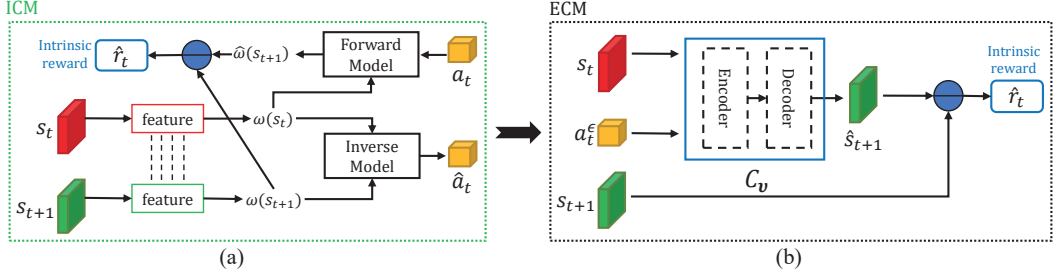


Figure 2: The architecture of ICM and ECM with $\omega(\cdot)$ denoting the encoding operation for the state space while \ominus being the Euclidean distance. Note that the encoder and decoder represent the two parts of the network responsible for downsampling and upsampling, respectively.

To provide effective and robust IRS, we propose a novel ECM with the following two improvements as compared to the conventional ICM. First, ICM requires encoding the state space, which will be difficult and produces much variance in the high-dimension state space. In contrast, our proposed ECM can overcome this problem by employing the end-to-end training without the necessity of encoding the state space. Second, the conventional ICM used two modules to reconstruct the transition process, which incurs high computational complexity. To circumvent this problem, the proposed ECM only uses one DNN to accept states and actions as input before directly generating the predicted next-states \hat{s}_{t+1} at the output. In particular, we utilize an ϵ -greedy action a_t^ϵ for discrete action space, which directs ECM to explore more state-action pairs for better generalization capability:

$$P(a_t^\epsilon) = \begin{cases} \frac{\epsilon}{|\mathcal{A}|}, & \text{if } a_t^\epsilon \neq a_t, \\ 1 - \epsilon + \frac{\epsilon}{|\mathcal{A}|}, & \text{if } a_t^\epsilon = a_t, \end{cases} \quad (9)$$

where $P(\cdot)$ denotes the probability and $|\mathcal{A}|$ is the cardinality of the action space.

During the ECM training, the ϵ -greedy method in Eq. (9) will randomly select an action from \mathcal{A} to replace the original action with a probability of ϵ . Given a trajectory $\tau = (s_0, a_0, \dots, a_{T-1}, s_T)$, we represent ECM denoted by C_v with a DNN with parameters v . Then, ECM is trained to minimize the following loss function:

$$L(v) = \sum_{t=0}^{T-1} \frac{1}{2} \|C_v(s_t, a_t^\epsilon) - s_{t+1}\|_2^2 + \frac{\lambda}{2} \|v\|_2^2, \quad (10)$$

where the second item is the regularization item to prevent overfitting. Finally, the resulting IRS takes the following form without the encoding operation:

$$\hat{r}_v(s_t, a_t, s_{t+1}) = \frac{1}{2} \|C_v(s_t, a_t) - s_{t+1}\|_2^2. \quad (11)$$

4.3 Hybrid Reward for BD Learning

After establishing ERB and IRB, we are ready to propose the following hybrid reward:

$$\tilde{r}(s_t, a_t, s_{t+1}) = \alpha \cdot \check{r}_\theta + \beta \cdot \hat{r}_v, \quad (12)$$

where $\alpha, \beta \in [0, 1]$ are the weighting coefficients of the extrinsic reward and the intrinsic reward, respectively. It should be emphasized that IRS and ERS should be normalized to the same range in practice.

Using the hybrid reward defined in Eq. (12), the generation policy $\hat{\pi}$ can be updated with any policy optimization method. Finally, the workflow of HAIRL is summarized in Algorithm 1.

5 Experimental Evaluation

In this section, we will evaluate the proposed HAIRL both on discrete and continuous control tasks of OpenAI Gym library and PyBullet library [34][35]. For benchmarking, several most representative

Algorithm 1 Hybrid Adversarial Inverse Reinforcement Learning

- 1: Collect demonstrations \mathcal{D} ;
- 2: Initialize the generation policy network $\hat{\pi}$, discriminator D_δ and ECM C_v ;
- 3: Initialize the coefficients α, β, ϵ and λ ;
- 4: **for** epoch $\ell = 1, \dots, E$ **do**
- 5: Execute policy $\hat{\pi}$ and collect the trajectory $\tau_\ell = (s_0, a_0, \dots, a_{T-1}, s_T)$;
- 6: Use \mathcal{D} and τ_ℓ to train the discriminator by minimizing the following loss function:
$$L(\delta) = \sum_{i=0}^{T-1} \mathbb{E}_{\hat{\pi}(\tau)}[D_\delta(s_t, a_t)] - \sum_{i=0}^{T-1} \mathbb{E}_{\mathcal{D}}[D_\delta(s_t, a_t)];$$
- 7: Use τ_ℓ to train ECM by minimizing the following loss function:
$$L(v) = \sum_{t=0}^{T-1} \frac{1}{2} \|C_v(s_t, a_t) - s_{t+1}\|_2^2 + \frac{\lambda}{2} \|v\|_2^2;$$
- 8: Calculate the hybrid reward for each state-action pair in τ_ℓ :
$$\tilde{r}(s, a, s') = \alpha \cdot \mathbb{E}_{\hat{\pi}(\tau)}[D_\delta(s, a)] + \beta \cdot \frac{1}{2} \|C_v(s, a) - s'\|_2^2;$$
- 9: Update $\hat{\pi}$ with respect to the hybrid reward using any policy optimization method.
- 10: **end for**

algorithms are carefully selected, including GIRIL, TREX, AIRL and the curiosity-driven imitation learning (CDIL) reported in [8]. The first two methods are two-stage BD-IRL algorithms, while the latter two belong to the imitation learning algorithms. With GIRIL and TREX, we can compare the efficiency between the one-stage and the two-stage algorithms. With AIRL and CDIL, we can validate that the HAIRL can imitate and outperform the demonstrator. For fair comparison, all these methods use the same architecture for the policy network.

5.1 Atari Games

We first evaluate the HAIRL on Atari games with discrete action space. The state space of Atari games is composed of images, which can be used to validate the robustness of HAIRL in high-dimensional state space. The selected games and detailed experimental setup can be found in Appendix C.

We show the results using the Space Invaders game as an example. Fig. 3 illustrates the variation of four metrics in training. As shown, the WD between demonstrator and generation policy decreased steadily, which implies that the generation policy is approaching the demonstrator as the training process proceeds. Meanwhile, it took only a few epochs for IRB to reach its convergence, which confirms the high efficiency of the proposed ECM. Finally, the average return and episode length of the agent also improved consistently as the agent was able to survive longer time and achieve higher performance in the game.

Next, we compare the performance of HAIRL against the existing algorithms. We use the normalized average one-life return as the key performance indicator (KPI), in which the reward values are normalized into $[0, 1]$ and the agent interacts with the environments initialized by 5 random seeds. Table 1 illustrates the performance comparison of HAIRL and benchmarks, in which the BD performance is shown in bold numbers. For instance, the value of "33.8/616" in the first row and first column means the algorithm takes 616 average steps to achieve a average return of 33.8.

As shown in Table 1, HAIRL successfully outperformed the expert in five games, producing an average performance gain of 13.72. In contrast, TREX and GIRIL outperformed the expert agent in four and two games, respectively. For the imitation algorithms CDIL and AIRL, CDIL achieved the BD performance in only one game, while AIRL failed to exceed the expert in all games. In the Q*Bert game, all algorithms failed to outperform the expert with the proposed HAIRL achieving the highest score. With a simpler architecture and less computation, HAIRL exhibited higher efficiency

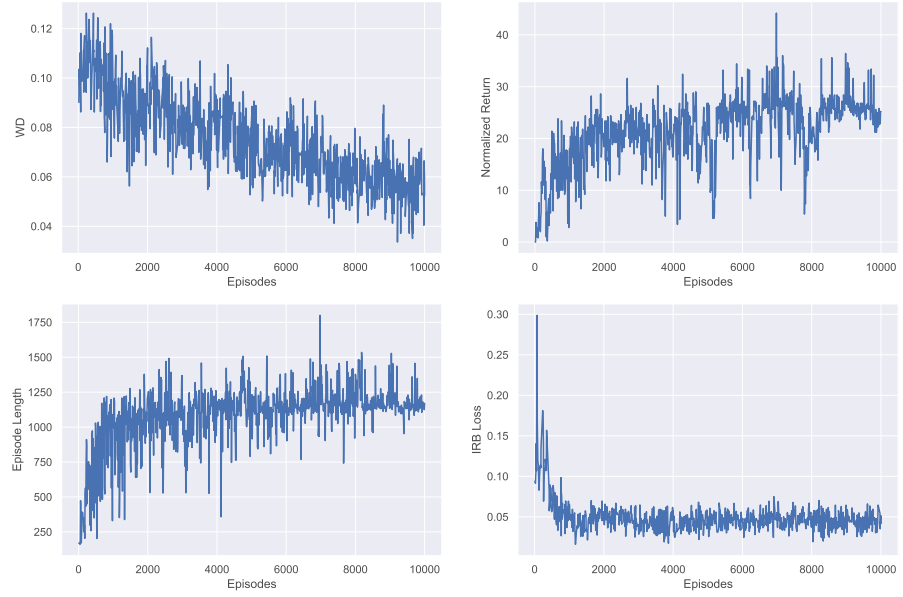


Figure 3: Training process of the Space Invaders game.

Table 1: Average return comparison in Atari games.

Game	Expert	One-stage		Two-stage		
	Average	HARIL	AIRL	GIRIL	CDIL	TREX
Space Invaders	33.8/616	36.4/1443	17.0/330	19.6/1043	25.2/1123	32.2/1441
Breakout	51.8/1134	60.2/1485	0.8/49	37.6/1021	56.4/1211	53.0/1207
Beam Rider	18.2/2057	50.0/5604	6.8/987	44.7/4095	2.8/1616	28.8/8934
Q*Bert	121.8/733	77.6/12116	3.7/141	30.7/56550	22.6/10905	43.0/7892
Kung Fu Master	28.2/671	51.8/1541	0.5/241	42.4/1391	12.6/569	40.6/1226
Seaquest	12.0/559	14.2/808	1.0/153	9.0/510	9.8/559	13.1/757

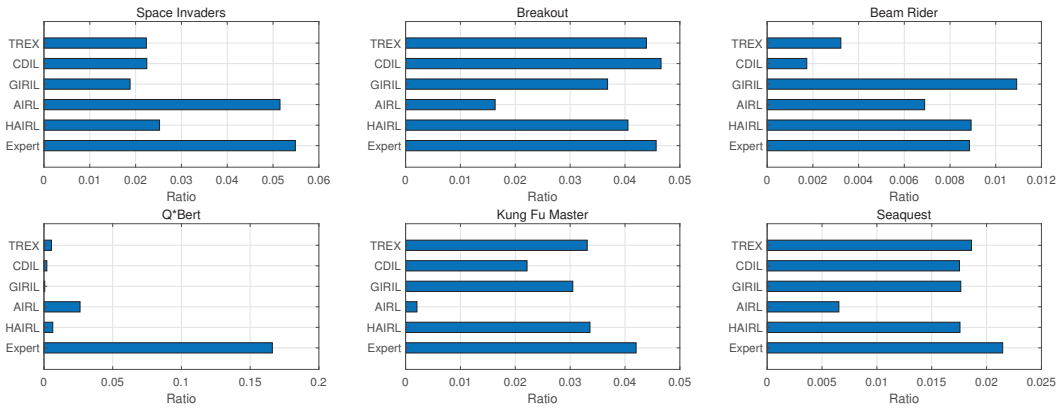


Figure 4: The ratio between the average return and the average steps required.

and better performance. Furthermore, we calculated the ratio between the average return and the average steps required as shown in Fig. 4. As compared to other curiosity-driven RL agents including the proposed HAIRL, the experts achieved a higher ratio in most games, especially in the Q*Bert game. In other words, the experts could attain the same performance with fewer steps, which is also observed in [36] and coined as the “procrastination” of the curiosity-driven RL agent. This is because the curiosity-driven RL agents spent larger efforts in exploring all possible states even though some states are useless. Therefore, these curiosity-driven RL agents usually achieved the same performance at the cost of more steps as compared to the expert. In HAIRL, ERS could lead the agent to imitate the expert policy and correct the influence of IRS. For instance, if a transition produces a high IRS and a high ERB instantaneously, ERB can intensify the motivation of the agent to explore the high-potential states. On the opposite, if the agent wastes much time on the same states, ERS will prevent the agent from visiting these states by reducing the rewards. In summary, HAIRL is more adaptive and robust when handling complex conditions.

5.2 PyBullet Games

Furthermore, we evaluate the HAIRL on PyBullet games with continuous action space. The selected games and detailed experimental setup can be found in Appendix D. We use the unnormalized

Table 2: Average return comparison in PyBullet games.

Game	Expert	One-stage		Two-stage		
	Average	HAIRL	AIRL	GIRIL	CDIL	TREX
Inverted Pendulum	821.7/821	844.4/844	754.7/754	835.3/835	823.6/823	833.1/833
Inverted Double Pendulum	903.9/97	918.9/98	856.3/80	915.5/96	905.5/96	912.4/95

average one-life return as the KPI, and the agent also interacts with the environments initialized by 5 random seeds. As shown in Table 2, HAIRL successfully outperformed the experts in all the games, producing the highest average performance gain of 18.85. GIRIL, CDIL, and TREX also outperformed the expert, while AIRL failed in all games again. The simulation results show that HAIRL can adapt to discrete and continuous control tasks, which provides powerful BD extrapolation ability with simpler architecture and lower computation complexity.

6 Conclusion

In this paper, we have investigated the problem of the BD-IRL. To realize efficient and robust BD-IRL, we propose a one-stage, GA fashion and curiosity-driven framework called the hybrid adversarial inverse reinforcement learning (HAIRL) that integrates the reward function learning and policy optimization into one procedure. As a result, the proposed HAIRL utilizes two modules, namely ERB and IRB, to collectively generate hybrid rewards for the agent to simultaneously imitate the demonstrator and extrapolate BD performance. Extensive simulation using multiple Atari games and PyBullet games was performed to confirm that the proposed HAIRL outperforms the conventional BD-IRL algorithms. Finally, we have not optimized the algorithm additionally for the continuous control tasks, which will be further improved in future research.

References

- [1] David Silver, Thomas Hubert, Julian Schrittwieser, Ioannis Antonoglou, Matthew Lai, Arthur Guez, Marc Lanctot, Laurent Sifre, Dharshan Kumaran, Thore Graepel, et al. A general reinforcement learning algorithm that masters chess, shogi, and go through self-play. *Science*, 362(6419):1140–1144, 2018.
- [2] Oriol Vinyals, Igor Babuschkin, Wojciech M Czarnecki, Michaël Mathieu, Andrew Dudzik, Junyoung Chung, David H Choi, Richard Powell, Timo Ewalds, Petko Georgiev, et al. Grandmaster level in starcraft ii using multi-agent reinforcement learning. *Nature*, 575(7782):350–354, 2019.
- [3] Andrew Y Ng, Daishi Harada, and Stuart Russell. Policy invariance under reward transformations: Theory and application to reward shaping. In *Icml*, volume 99, pages 278–287, 1999.

- [4] Bradly C Stadie, Sergey Levine, and Pieter Abbeel. Incentivizing exploration in reinforcement learning with deep predictive models. *arXiv preprint arXiv:1507.00814*, 2015.
- [5] Andrew Y Ng, Stuart J Russell, et al. Algorithms for inverse reinforcement learning. In *Icml*, volume 1, page 2, 2000.
- [6] Richard S Sutton and Andrew G Barto. *Reinforcement learning: An introduction*. MIT press, 2018.
- [7] Daniel S Brown, Wonjoon Goo, Prabhat Nagarajan, and Scott Niekum. Extrapolating beyond suboptimal demonstrations via inverse reinforcement learning from observations. *arXiv preprint arXiv:1904.06387*, 2019.
- [8] Xingrui Yu, Yueming Lyu, and Ivor Tsang. Intrinsic reward driven imitation learning via generative model. In *International Conference on Machine Learning*, pages 10925–10935. PMLR, 2020.
- [9] Sili Huang, Bo Yang, Hechang Chen, Haiyin Piao, Zhixiao Sun, and Yi Chang. Ma-trex: Multi-agent trajectory-ranked reward extrapolation via inverse reinforcement learning. In *International Conference on Knowledge Science, Engineering and Management*, pages 3–14. Springer, 2020.
- [10] Daniel S Brown, Wonjoon Goo, and Scott Niekum. Better-than-demonstrator imitation learning via automatically-ranked demonstrations. In *Conference on Robot Learning*, pages 330–359. PMLR, 2020.
- [11] Diederik P Kingma and Max Welling. Auto-encoding variational bayes. *arXiv preprint arXiv:1312.6114*, 2013.
- [12] Brian D Ziebart, Andrew L Maas, J Andrew Bagnell, and Anind K Dey. Maximum entropy inverse reinforcement learning. In *Aaai*, volume 8, pages 1433–1438. Chicago, IL, USA, 2008.
- [13] Brian D Ziebart. Modeling purposeful adaptive behavior with the principle of maximum causal entropy. 2010.
- [14] Deepak Ramachandran and Eyal Amir. Bayesian inverse reinforcement learning. In *IJCAI*, volume 7, pages 2586–2591, 2007.
- [15] Dylan Hadfield-Menell, Anca Dragan, Pieter Abbeel, and Stuart Russell. Cooperative inverse reinforcement learning. *arXiv preprint arXiv:1606.03137*, 2016.
- [16] Sergey Levine, Zoran Popovic, and Vladlen Koltun. Nonlinear inverse reinforcement learning with gaussian processes. *Advances in neural information processing systems*, 24:19–27, 2011.
- [17] Markus Wulfmeier, Peter Ondruska, and Ingmar Posner. Deep inverse reinforcement learning. *arXiv preprint arXiv:1507.04888*, 2015.
- [18] Kareem Amin, Nan Jiang, and Satinder Singh. Repeated inverse reinforcement learning. *arXiv preprint arXiv:1705.05427*, 2017.
- [19] Sriraam Natarajan, Gautam Kunapuli, Kshitij Judah, Prasad Tadepalli, Kristian Kersting, and Jude Shavlik. Multi-agent inverse reinforcement learning. In *2010 Ninth International Conference on Machine Learning and Applications*, pages 395–400. IEEE, 2010.
- [20] Chelsea Finn, Paul Christiano, Pieter Abbeel, and Sergey Levine. A connection between generative adversarial networks, inverse reinforcement learning, and energy-based models. *arXiv preprint arXiv:1611.03852*, 2016.
- [21] Ian Goodfellow, Jean Pouget-Abadie, Mehdi Mirza, Bing Xu, David Warde-Farley, Sherjil Ozair, Aaron Courville, and Yoshua Bengio. Generative adversarial nets. *Advances in neural information processing systems*, 27:2672–2680, 2014.
- [22] Justin Fu, Katie Luo, and Sergey Levine. Learning robust rewards with adversarial inverse reinforcement learning. *arXiv preprint arXiv:1710.11248*, 2017.
- [23] Pierre-Yves Oudeyer and Frederic Kaplan. What is intrinsic motivation? a typology of computational approaches. *Frontiers in neurorobotics*, 1:6, 2009.
- [24] Marc Bellemare, Sriram Srinivasan, Georg Ostrovski, Tom Schaul, David Saxton, and Remi Munos. Unifying count-based exploration and intrinsic motivation. *Advances in neural information processing systems*, 29:1471–1479, 2016.

[25] Manuel Lopes, Tobias Lang, Marc Toussaint, and Pierre-Yves Oudeyer. Exploration in model-based reinforcement learning by empirically estimating learning progress. In *Advances in neural information processing systems*, pages 206–214, 2012.

[26] Rein Houthooft, Xi Chen, Yan Duan, John Schulman, Filip De Turck, and Pieter Abbeel. Vime: Variational information maximizing exploration. *Advances in neural information processing systems*, 29:1109–1117, 2016.

[27] Yi Sun, Faustino Gomez, and Jürgen Schmidhuber. Planning to be surprised: Optimal bayesian exploration in dynamic environments. In *International Conference on Artificial General Intelligence*, pages 41–51. Springer, 2011.

[28] Satinder Singh, Andrew G Barto, and Nuttapong Chentanez. Intrinsically motivated reinforcement learning. Technical report, MASSACHUSETTS UNIV AMHERST DEPT OF COMPUTER SCIENCE, 2005.

[29] Deepak Pathak, Pulkit Agrawal, Alexei A Efros, and Trevor Darrell. Curiosity-driven exploration by self-supervised prediction. In *Proceedings of the IEEE Conference on Computer Vision and Pattern Recognition Workshops*, pages 16–17, 2017.

[30] Yuri Burda, Harri Edwards, Deepak Pathak, Amos Storkey, Trevor Darrell, and Alexei A Efros. Large-scale study of curiosity-driven learning. *arXiv preprint arXiv:1808.04355*, 2018.

[31] Martin Arjovsky and Léon Bottou. Towards principled methods for training generative adversarial networks. *arXiv preprint arXiv:1701.04862*, 2017.

[32] Martin Arjovsky, Soumith Chintala, and Léon Bottou. Wasserstein gan. *arXiv preprint arXiv:1701.07875*, 2017.

[33] Cédric Villani. *Optimal transport: old and new*, volume 338. Springer Science & Business Media, 2008.

[34] Greg Brockman, Vicki Cheung, Ludwig Pettersson, Jonas Schneider, John Schulman, Jie Tang, and Wojciech Zaremba. Openai gym. *arXiv preprint arXiv:1606.01540*, 2016.

[35] Erwin Coumans and Yunfei Bai. Pybullet, a python module for physics simulation for games, robotics and machine learning. <http://pybullet.org>, 2016–2021.

[36] Nikolay Savinov, Anton Raichuk, Raphaël Marinier, Damien Vincent, Marc Pollefeys, Timothy Lillicrap, and Sylvain Gelly. Episodic curiosity through reachability. *arXiv preprint arXiv:1810.02274*, 2018.

[37] Yann LeCun, Sumit Chopra, Raia Hadsell, M Ranzato, and F Huang. A tutorial on energy-based learning. *Predicting structured data*, 1(0), 2006.

[38] Yann LeCun, Yoshua Bengio, and Geoffrey Hinton. Deep learning. *nature*, 521(7553):436–444, 2015.

[39] Alexander Shapiro. Monte carlo sampling methods. *Handbooks in operations research and management science*, 10:353–425, 2003.

[40] Wassily Hoeffding. Probability inequalities for sums of bounded random variables. In *The Collected Works of Wassily Hoeffding*, pages 409–426. Springer, 1994.

[41] John Schulman, Filip Wolski, Prafulla Dhariwal, Alec Radford, and Oleg Klimov. Proximal policy optimization algorithms. *arXiv preprint arXiv:1707.06347*, 2017.

[42] Kostrikov. Pytorch implementation of the reinforcement learning algorithms. URL <https://github.com/ikostrikov/pytorch-a2c-ppo-acktr-gail>, 2018.

[43] Diederik P Kingma and Jimmy Ba. Adam: A method for stochastic optimization. *arXiv preprint arXiv:1412.6980*, 2014.

A Proof of Theorem 1

ERB simply aims to imitate the demonstrator policy, which is consistent with the objective defined in Eq. (2). Let:

$$\max_{\boldsymbol{\theta}} I(\boldsymbol{\theta}) = \max_{\boldsymbol{\theta}} \mathbb{E}_{\tau \sim \mathcal{D}} [\log p_{\boldsymbol{\theta}}(\tau)],$$

where $p_{\boldsymbol{\theta}}(\tau) \propto \rho(s_0) \prod_{t=0}^{T-1} \mathcal{T}(s_{t+1}|s_t, a_t) e^{\gamma^t r_{\boldsymbol{\theta}}(s_t, a_t)}$. The demonstrations satisfy the Boltzmann distribution [12][37]:

$$p_{\boldsymbol{\theta}}(\tau) = \frac{1}{Z_{\boldsymbol{\theta}}} \exp \left\{ \sum_{(s_t, a_t) \in \tau} r_{\boldsymbol{\theta}}(s_t, a_t) \right\} = \frac{1}{Z_{\boldsymbol{\theta}}} \tilde{p}_{\boldsymbol{\theta}}(\tau),$$

where $\tilde{p}_{\boldsymbol{\theta}}$ is the probability distribution before normalization and $Z_{\boldsymbol{\theta}} = \int_{\tau} \tilde{p}_{\boldsymbol{\theta}}(\tau) d\tau$ is the partition function. Taking the gradient of the $I(\boldsymbol{\theta})$ with respect to $\boldsymbol{\theta}$, we have:

$$\nabla_{\boldsymbol{\theta}} I(\boldsymbol{\theta}) = \mathbb{E}_{\mathcal{D}} [\nabla_{\boldsymbol{\theta}} \log p_{\boldsymbol{\theta}}(\tau)] = \mathbb{E}_{\mathcal{D}} \left[\sum_{t=0}^{T-1} \nabla_{\boldsymbol{\theta}} r_{\boldsymbol{\theta}}(s_t, a_t) \right] - \nabla_{\boldsymbol{\theta}} \log Z_{\boldsymbol{\theta}}.$$

In [38], it has been proved that the gradient of $Z_{\boldsymbol{\theta}}$ satisfies:

$$\nabla_{\boldsymbol{\theta}} \log Z_{\boldsymbol{\theta}} = \mathbb{E}_{p_{\boldsymbol{\theta}}} \nabla_{\boldsymbol{\theta}} \log \tilde{p}_{\boldsymbol{\theta}}.$$

Therefore, the gradient can be written as:

$$\begin{aligned} \nabla_{\boldsymbol{\theta}} I(\boldsymbol{\theta}) &= \mathbb{E}_{\mathcal{D}} \left[\sum_{t=0}^{T-1} \nabla_{\boldsymbol{\theta}} r_{\boldsymbol{\theta}}(s_t, a_t) \right] - \mathbb{E}_{p_{\boldsymbol{\theta}}} \left[\sum_{t=0}^{T-1} \nabla_{\boldsymbol{\theta}} r_{\boldsymbol{\theta}}(s_t, a_t) \right], \\ &= \sum_{t=0}^{T-1} \left(\mathbb{E}_{\mathcal{D}} [\nabla_{\boldsymbol{\theta}} r_{\boldsymbol{\theta}}(s_t, a_t)] - \mathbb{E}_{p_{\boldsymbol{\theta}, t}} [\nabla_{\boldsymbol{\theta}} r_{\boldsymbol{\theta}}(s_t, a_t)] \right), \end{aligned} \quad (13)$$

where $p_{\boldsymbol{\theta}, t}(s_t, a_t) = \int_{s_{t'} \neq t} \int_{a_{t'} \neq t} p_{\boldsymbol{\theta}}(\tau) ds_{t'} da_{t'}$ is the state-action marginal at time t . Since it is difficult to directly obtain samples from $p_{\boldsymbol{\theta}, t}$, we apply the importance sampling method to estimate its expectation [39]. Finally, the gradient can be rewritten as follows:

$$\nabla_{\boldsymbol{\theta}} I(\boldsymbol{\theta}) = \sum_{t=0}^{T-1} \left(\mathbb{E}_{\mathcal{D}} [\nabla_{\boldsymbol{\theta}} r_{\boldsymbol{\theta}}(s_t, a_t)] - \mathbb{E}_{\mu_t} \left[\frac{p_{\boldsymbol{\theta}, t}(s_t, a_t)}{\mu_t(s_t, a_t)} \nabla_{\boldsymbol{\theta}} r_{\boldsymbol{\theta}}(s_t, a_t) \right] \right), \quad (14)$$

where $\mu(\tau) = \rho(s_0) \prod_{t=0}^{T-1} \mathcal{T}(s_{t+1}|s_t, a_t) \mu(a_t|s_t)$ is the sampling distribution.

Furthermore, we propose to design the sampler to reduce the variance of importance sampling. Recalling the definition of $p_{\boldsymbol{\theta}}(\tau)$, the optimal sampling distribution satisfies:

$$\mu_{\tau} \propto \exp \left\{ \sum_{(s_t, a_t) \in \tau} r_{\boldsymbol{\theta}}(s_t, a_t) \right\}.$$

Thus, the sampler $\mu(s_t, a_t)$ is designed to maximize the following objective function to approximate the demonstrator policy:

$$\mathbb{E}_{\tau \sim \mu(\tau)} \left[\sum_{t=0}^{T-1} \gamma^t r_{\boldsymbol{\theta}}(s_t, a_t) \right]. \quad (15)$$

Therefore, $\mu(a|s)$ can imitate the demonstrator policy by alternatively optimizing Eq. (14) and Eq. (15).

Next, we observe the loss function shown in Eq. (6). The gradient of its opposite form is given by:

$$\nabla_{\boldsymbol{\delta}} L(\boldsymbol{\delta}) = \sum_{t=0}^{T-1} \left(\mathbb{E}_{\mathcal{D}} [\nabla_{\boldsymbol{\delta}} D_{\boldsymbol{\delta}}(s_t, a_t)] - \mathbb{E}_{\hat{p}_t} [\nabla_{\boldsymbol{\delta}} D_{\boldsymbol{\delta}}(s_t, a_t)] \right), \quad (16)$$

where $\hat{p}_t(s_t, a_t)$ is the state-action marginal induced by $\hat{\pi}$. Note that Eq. (16) is consistent with Eq. (14) when $D_{\boldsymbol{\sigma}}(s, a)$ serves as the reward function. After the discriminator is updated, $\hat{\pi}$ is designed to maximize the same objective as shown in Eq. (15). Therefore, the learning process of ERB and MLE is consistent. This concludes the proof.

B Proof of Theorem 2

We first define a set \mathcal{F} of Lipschitz-1 functions for two policy $\pi, \pi' \in \Pi, \pi \neq \pi'$ with

$$f := \operatorname{argmax}_{\|f\|_L \leq 1} \left[\mathbb{E}_{s,a \sim \pi}[f(s,a)] - \mathbb{E}_{s,a \sim \pi'}[f(s,a)] \right], \quad (17)$$

where $f \in \mathcal{F}, |\mathcal{F}| \leq |\Pi|^2$. Given the trajectory set \mathcal{D} that contains M state-action pairs, minimizing the WD between $\hat{\pi}$ and \mathcal{D} is equivalent to the following optimization problem:

$$\hat{\pi} = \operatorname{argmin}_{\pi \in \Pi} \left[\max_{f \in \mathcal{F}} \left[\frac{1}{M} \sum_{i=1}^M f(s_i, a_i) - \mathbb{E}_{s,a \sim \pi} f(s,a) \right] \right], \quad (18)$$

where $(s_i, a_i) \in \mathcal{D}$ and $\frac{1}{M} \sum_{i=1}^M f(s_i, a_i)$ is the estimation of the $\mathbb{E}_{s,a \sim \mathcal{D}} f(s,a)$. Capitalizing on the Hoeffding's inequality [40] for all $f \in \mathcal{F}$, we have

$$\left| \frac{1}{M} \sum_{i=1}^M f(s_i, a_i) - \mathbb{E}_{s,a \sim \mathcal{D}} f(s,a) \right| \leq 2 \sqrt{\frac{\ln(|\mathcal{F}|/\kappa)}{M}} = \epsilon.$$

Next, we define \hat{f} and \tilde{f} as follows:

$$\begin{aligned} \hat{f} &:= \operatorname{argmax}_{f \in \mathcal{F}} \left[\mathbb{E}_{s,a \sim \mathcal{D}}[f(s,a)] - \mathbb{E}_{s,a \sim \hat{\pi}}[f(s,a)] \right], \\ \tilde{f} &:= \operatorname{argmax}_{f \in \mathcal{F}} \left[\frac{1}{M} \sum_{i=1}^M f(s_i, a_i) - \mathbb{E}_{s,a \sim \hat{\pi}} f(s,a) \right]. \end{aligned}$$

We can have the following inequalities:

$$\begin{aligned} \max_{\|f\|_L \leq 1} \mathbb{E}_{s,a \sim \mathcal{D}}[f(s,a)] - \mathbb{E}_{s,a \sim \hat{\pi}}[f(s,a)], \\ &= \mathbb{E}_{s,a \sim \mathcal{D}}[\hat{f}(s,a)] - \mathbb{E}_{s,a \sim \hat{\pi}}[\hat{f}(s,a)], \\ &\leq \epsilon + \frac{1}{M} \sum_{i=1}^M \tilde{f}(s_i, a_i) - \mathbb{E}_{s,a \sim \hat{\pi}}[\tilde{f}(s,a)], \\ &\leq \epsilon + \frac{1}{M} \sum_{i=1}^M \tilde{f}(s_i, a_i) - \mathbb{E}_{s,a \sim \mathcal{D}}[\tilde{f}(s,a)], \\ &\leq 2\epsilon \leq 4\sqrt{\frac{2 \ln(|\Pi|) - \ln(\kappa)}{M}}, \end{aligned}$$

where the second inequality follows the fact that $\hat{\pi}$ is the minimizer of Eq. (18). This concludes the proof.

C Experimental Setup for Atari Games

C.1 Expert Demonstrations

Table 3 illustrates the details of the selected games. To generate the expert demonstrations, we used the proximal policy optimization (PPO) to train expert agents with the true reward [41]. The agent was set to interact with the environment for ten million steps. More specifically, we used the PyTorch implementation of the PPO created by [42] while other hyperparameters were set as default. After the expert agents were established, they were used to generate demonstrations with randomly initialized environments.

C.2 Experimental Setup

Since the state space of the Atari games is composed of images, convolutional neural networks (CNNs) were used to build HAIRL. Table 4 illustrates the detailed architectures employed in our

Table 3: The details of the Atari games.

Game	Observation shape	Action space size
Breakout	(84,84,4)	4
Space Invaders	(84,84,4)	6
Q*Bert	(84,84,4)	6
Beam Rider	(84,84,4)	9
Kung Fu Master	(84,84,4)	14
Seaquest	(84,84,4)	18

Table 4: The CNN-based architecture of the modules.

Module	$\hat{\pi}$	D_δ	C_v
Input	States	States and one-hot actions	States and one-hot actions
Arch.	8×8 Conv 32, ReLU	8×8 Conv 32, Tanh	8×8 Conv 32, ReLU
	4×4 Conv 64, ReLU	4×4 Conv 64, Tanh	4×4 Conv 64, ReLU
	3×3 Conv 32, ReLU	3×3 Conv 32, Tanh	3×3 Conv 32, ReLU
	Flatten	Flatten	Flatten
	Dense 512, ReLU	Dense 128, Tanh	Dense 32*11*11
	Dense $ \mathcal{A} $	Dense 1	Reshape to (32,11,11)
	Categorical Distribution		ConvTranspose 32, ReLU
Output	Actions	Scores	ConvTranspose 32, ReLU
			ConvTranspose 32

experiments, where each convolutional layer is followed by a batch normalization (BN) layer while the Flatten layer is used to convert a tensor into a vector. Finally, ConvTranspose is a special convolutional operation for upsampling.

We trained HAIRL for ten thousand epochs. In each epoch, the agent interacts with eight parallel environments for 128 steps, producing 1024 pieces of transitions. Firstly, the transitions are leveraged to update the discriminator D_δ . More specifically, the batch size is set as 256, and the RMSprop optimizer was used to apply the gradient descent with a linearly decaying learning rate. In particular, the gradients and weights were clipped into $[-5, 5]$ and $[-0.1, 0.1]$. It satisfied the requirement for approximating the WD and stabilizing the training process. Secondly, we used the generated transitions to train ECM that accepted an image of size (84, 84, 4) before downsampling the image to produce a feature vector. After that, the feature vector was concatenated with the one-hot action that was processed by the latter part of C_v to regenerate an image of size (84, 84, 4). The batch size was set to 256, $\epsilon = 0.1$, $\lambda = 0.01$ while the learning rate also decayed linearly. However, we used the Adam optimizer reported in [43] to apply the gradient descent.

After ERB and IRB were updated, they were used to calculate the hybrid rewards for the transitions, where $\alpha = 0.01$ and $\beta = 0.99$. The PPO then accepted the transitions with hybrid rewards to update the generation policy $\hat{\pi}$. As for the training of the benchmark algorithms, we follow the default settings reported in the literature.

D Experimental Setup for PyBullet Games

D.1 Expert Demonstrations

Table 5 illustrates the details of the selected games. To generate the expert demonstrations, we also used the PPO to train expert agents. The agent was set to interact with the environment for five million steps. After the expert agents were established, they were used to generate demonstrations with randomly initialized environments.

Table 5: The details of the PyBullet games.

Game	Observation shape	Action space size
Inverted Pendulum	(1,5)	[-1,+1]
Inverted Double Pendulum	(1,9)	[-1,+1]

D.2 Experimental Setup

The observation of the PyBullet games is a fixed-length vector with real numbers, so we use the multilayer perceptron (MLP) to build HAIRL. Since we do not need to conduct complex downsampling and upsampling operations like the Atari games, simple network architecture is sufficient for the algorithm. Table 6 illustrates the detailed architectures employed in our experiments.

Table 6: The MLP-based architectures of the modules.

Module	$\hat{\pi}$	D_δ	C_v
Input	States	States and actions	States and actions
Arch.	Dense 64, Tanh	Dense 64, ReLU	Dense 64, ReLU
	Dense 64, Tanh	Dense 128, ReLU	Dense 128, ReLU
	Dense Action shape	Dense 1	Dense Observataion shape
	Gaussian Distribution		
Output	Actions	Scores	Predicted next-states

We also trained HAIRL for ten thousand epochs. In each epoch, the agent interacts with eight parallel environments for 128 steps, producing 1024 pieces of transitions. After that, the training procedure and hyperparameters of ERB and IRB are same with Appendix C. After ERB and IRB were updated, they were used to calculate the hybrid rewards for the transitions, where $\alpha = 0.5$ and $\beta = 0.5$. The PPO then accepted the transitions with hybrid rewards to update the generation policy $\hat{\pi}$. As for the training of the benchmark algorithms, we also follow the default settings reported in the literature.